Journal of Power Sources 196 (2011) 10496–10501

Contents lists available at SciVerse ScienceDirect

Journal of Power Sources

journal homepage: www.elsevier.com/locate/jpowsour

Solvent-induced porosity control of carbon nanofiber webs for supercapacitor

Bo-Hye Kim[a], Kap Seung Yang[a,b,*], Yoong Ahm Kim[c,**], Yong Jung Kim[d], Bai An[e], Kyoichi Oshida[f]

[a] Alan G. MacDiarmid Energy Research Institute, Chonnam National University, 300 Yongbong-dong, Buk-gu, Gwangju 500-757, Republic of Korea
[b] Department of Polymer & Fiber System Engineering, Chonnam National University, 300 Yongbong-dong, Buk-gu, Gwangju 500-757, Republic of Korea
[c] Faculty of Engineering Shinshu University, 4-17-1 Wakasato, Nagano-shi 380-8553, Japan
[d] Research Institute of Industrial Science & Technology, San 32, Hyoja-dong, Nam-gu, Pohang 790-600, Republic of Korea
[e] National Institute of Advanced Industrial Science and Technology, AIST East, 16-1 Onogawa, Tsukuba, Ibaraki 305-8569, Japan
[f] Department of Electronics and Computer Science, Nagano National College of Technology, Nagano 381-8550, Japan

ARTICLE INFO

Article history:
Received 19 July 2011
Received in revised form 17 August 2011
Accepted 17 August 2011
Available online 30 August 2011

Keywords:
Porosity
Skin–core
Electrospinning
Pore size distribution
Supercapacitor

ABSTRACT

A simple and scalable method is reported for fabricating a porosity-controlled carbon nanofibers with a skin–core texture by electrospinning a selected blend of polymer solutions. Simple thermal treatment of the electrospun nanofibers from solution blends of various compositions creates suitable ultramicropores on the surface of carbon nanofibers that can accommodate many ions, removing the need for an activation step. The intrinsic properties of the electrode (e.g., nanometre-size diameter, high specific surface area, narrow pore size distribution, tuneable porosity, shallow pore depth, and good ionic accessibility) enable construction of supercapacitors with large specific capacitance (130.7 F g^{-1}), high power (100 kW kg^{-1}), and energy density (15.0 Wh kg^{-1}).

1. Introduction

Due to their high power density and long life-time, electrochemical capacitors are promising power sources for portable electronic systems and automotive applications [1–3]. To improve the performance of these capacitors, several approaches have been investigated (e.g., controlling the pore size distribution, introducing electroactive metallic particles or electron conducting polymers, and fabricating hybrid-type cells) [4–6]. Among the many types of active materials, carbon nanofibers (CNFs) are of great practical importance due to their flexibility and high aspect ratio (above 10^6). Moreover, to improve the energy density and ion transport within electrode materials, thin films consisting of carbon nanotubes and CNFs have been suggested as promising flexible electrodes for supercapacitors [7–9]. In this work, we investigated this approach for improving energy storage efficiency by narrow distribution of pore sizes, which can enhance the ionic accessibility into the pores polyacrylonitrile (PAN)/pitch-based CNFs having a skin–core structure. Further, the size of pores formed in the surface of the fiber can be controlled to an appropriate degree.

2. Experimental

2.1. Fabrication

The pitch provided through condensation of the pyrolized fuel oil (PFO) with Cl_2 by Hanwha Chemical Co., Korea. The PFO used as the raw material is a heavy residual oil as by-product from naphtha cracking. The properties of the pitch used are summarized in Table 1. The concentration of pitch in THF was varied between 50 and 20 wt.%. A solution of PAN in DMF was added to pitch in THF solution to achieve a PAN/pitch weight ratio of 7/3 wt.%. To produce a web, a voltage of 20 kV was applied to the positively charged capillary, and a tip-to-collector distance of 25 cm was maintained during the electrospinning process. The nanofibers were stabilized in air and carbonized at 1000 °C in a horizontal furnace under a flow of nitrogen.

2.2. Characterization

The CNFs were characterized by SEM (Hitachi, S-4700, Japan), TEM (using JEOL JEM-2010 FEF), and nitrogen adsorption–desorption isotherms (ASAP2010, Micromeritics

* Corresponding author at: Department of Polymer & Fiber System Engineering, Chonnam National University, 300 Yongbong-dong, Buk-gu, Gwangju 500-757, Republic of Korea. Tel.: +82 62 530 0774; fax: +82 62 530 1779.
** Corresponding author at: Faculty of Engineering Shinshu University, 4-17-1 Wakasato, Nagano-shi 380-8553, Japan. Tel.: +81 26 269 5212; fax: +81 26 269 5208.
E-mail addresses: ksyang@chonnam.ac.kr (K.S. Yang), yak@endomoibu.shinshu-u.ac.jp (Y.A. Kim).

0378-7753/$ – see front matter © 2011 Elsevier B.V. All rights reserved.
doi:10.1016/j.jpowsour.2011.08.088

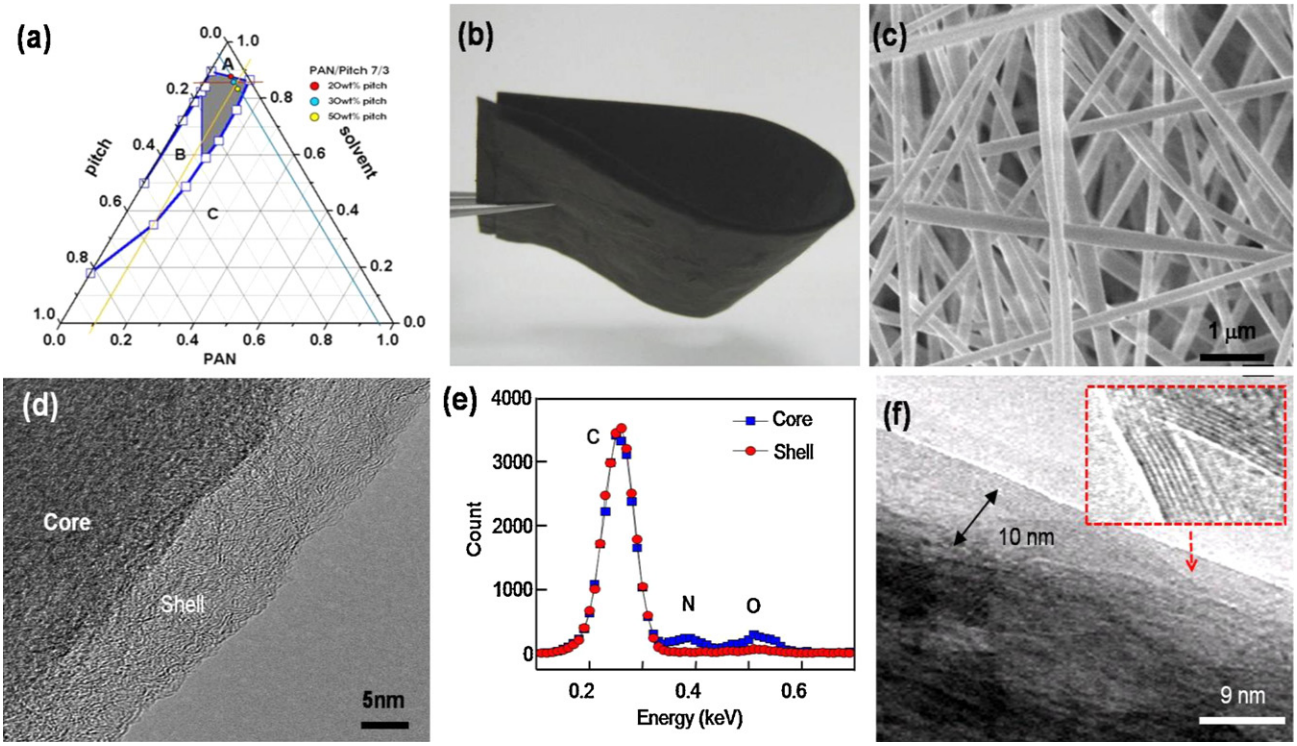

Fig. 1. (a) PAN–pitch–solvent ternary phase diagram. (b) Photograph showing a bendable CNFs. (c) SEM image of CNFs. (d) TEM image of CNFs. (e) EDX spectroscopy of air-stabilized nanofibers. (f) TEM of a CNFs thermally treated up to 2800 °C in argon.

Instruments Co.). The full range of pore sizes over a continuous scale was confirmed through density functional theory calculations (DFT PLUS for Windows). The microdomain structures of CNFs were confirmed by scanning tunneling microscopy (STM). STM images were acquired in a constant current mode with the current range of 0.2–1 nA, a bias voltage in the range of 0.1–1.0 V, and scan frequencies of 1–2 Hz using the Nanoscope III (Digital Instrument, CA). The electrical resistivity of an individual carbon nanofiber was measured according to the following procedure. After spin-coating a nanofiber suspension onto SiO_2 electrodes, the electrode patterns were formed by depositing TiO_2 on a carbon nanofiber via focused-ion-beam lithography (SMI2059, SII, Japan) to exclude the contact resistance between the carbon fiber and the electrode. The intrinsic resistivity was determined from the linear current–voltage relationship at −1 to 1 V (Advantest, TR-6143).

2.3. Electrochemical tests

Supercapacitor cells were built by assembling two 2.25 cm^2 electrodes separated by polypropylene separators (Cellgard 3501). The thickness of electrode is 0.08–1.00 mm. A nickel plate was attached to each side to collect the current on the surface of the electrode. The electrode consisted of a self-sustained porous CNF web and was constructed without using any binding or conductive materials. The electrode performance was measured in 6 M aqueous KOH at room temperature. Cyclic voltammetry (CV) of the unit cell was performed at potentials of 0–1.0 V by varying the scan rate from 10 to 100 mV s^{-1}. Eq. (1) was used to calculate the capacitance of the two-electrode system from the charge–discharge curves. The cell capacitance was calculated from the slope of the discharge based on Eq. (1);

$$C = i\left(\frac{\Delta t}{\Delta V}\right) \quad (1)$$

where C is the capacitance of the cell in farads (F), i is the discharge current in amperes (A), Δt is the discharging time from 0.6 to 0.5 V (approximately 60–50% of the initial voltage), ΔV is the voltage variation in the time range measured, and the slope in volts per second (V s^{-1}). In a symmetrical system, the specific capacitance

Table 1
Average molecular weight of the pitches determined by GPC.

	M_w [b]	M_n [c]	PDI (M_w/M_n)[d]
Pitch[a]	2380	1982	1.20

[a] THF soluble fraction.
[b] M_w, weight-average molecular weight.
[c] M_n, number-average molecular weight.
[d] PDI, polydispersity index.

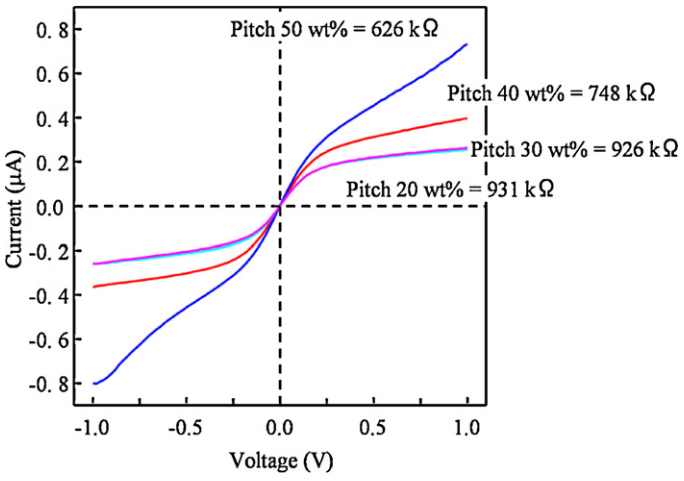

Fig. 2. The current–voltage profiles of single carbon nanofibers in the range from −1.0 to 1.0 V.

Table 2
Pore characteristics and electrical conductivity of PAN/pitch based CNFs.

I.D.	Pore property			Electrical conductivity	
	Specific surface area ($m^2\,g^{-1}$)	Pore volume ($cm^3\,g^{-1}$)	Average pore (Å)	Individual fiber resistance (kΩ)	Individual fiber conductivity ($S\,cm^{-1}$)
PAN/pitch = 7/3 (PC = 20)[a]	966.3	0.3788	15.73	931	3.96
PAN/pitch = 7/3 (PC = 30)[a]	887.2	0.3483	15.70	926	4.28
PAN/pitch = 7/3 (PC = 40)[a]	820.3	0.3550	15.78	748	2.09
PAN/pitch = 7/3 (PC = 50)[a]	692.9	0.2714	15.67	626	1.72
PAN	502.5	0.1654	16.99	845	1.29

[a] The pitch concentration in THF.

C_m in farads per gram of sample ($F\,g^{-1}$) is related to the specific capacitance of the cell, C, in terms of Eq. (2);

$$C_m = \frac{2C}{m} \tag{2}$$

where m is the weight (g) per electrode of samples.

The energy density was measured as a function of constant power discharge in the range of 400–100,000 $W\,kg^{-1}$. The ac impedance of the unit cell was measured at frequencies of 10 mHz–100 kHz using an electrochemical impedance analyzer (Jahner Electrik IM6, Germany). The ac impedance of the unit cell was measured at frequencies of 10 mHz–100 kHz using an electrochemical impedance analyzer.

3. Results and discussion

The PAN–pitch–solvent ternary phase diagram is presented in Fig. 1a. Phase A indicates the homogeneous solution, phase B denotes the biphasic solution whereas phase C indicates the mixture of solid solute and solvent. The shaded region in phase B denotes high spinnability, which is suitable for the formation of homogeneous nanofibers. Using a solution containing 30% of pitch, a bendable web (Fig. 1b) having an average diameter of 150 nm without any beads was produced (Fig. 1c). Noticeably, TEM image (Fig. 1d) shows that an individual CNF exhibits two-phase separation. Due to the noticeable difference in the molecular weight, the surface tension, and boiling point of DMF and THF, it is expected that the lighter phase would be pushed to the outer of fiber surface in the processes of solvent evaporation during electrospinning and heat-treatment [10]. Because of the substantial differences in the basic features of the two constituent polymers in solution, the low molecular weight pitch was preferentially located in the shell [11]. As a result of observing two phases using EDX, the presence of nitrogen and oxygen was confirmed in the core and only carbon was confirmed in the skin of the air-stabilized fibers in Fig. 1e. This stabilized fiber was obtained by diffusing oxygen from the air into the fiber so that oxygen was condensed with the heterogeneous element to cyclize PAN or form a network with nitrogen atoms, resulting in a flame-resistant material. The absence of nitrogen and oxygen atoms in the shell can be explained by the nature of pitch and the dehydration reaction of the diffused and adsorbed oxygen atoms. In order to observe the phase dispersion clearly, CNFs prepared at a temperature of 1000 °C in argon were thermally treated up to 2800 °C using a graphite furnace. As shown in Fig. 1f, two phases and well-developed crystalline layers in the skin of the fiber were observed.

To characterize the pore structures of CNFs, the pitch concentration in THF was varied from 20 to 50 wt.%. As summarized in Table 2, the specific surface area, pore volume, and average pore size proportional increased with decreasing the pitch concentration, because THF has a lower boiling point than DMF and evaporates more readily at lower temperatures. We measured the electrical resistivity of an individual CNF (the electrical resistivity in the bulk state was determined from the contact resistivity between the fibers and the intrinsic resistivity of individual fibers). All of the samples exhibited ohmic behavior, and the electrical resistivity of an individual CNF was between 600 and 1000 kΩ at room temperature, as shown in Fig. 2. The electrical conductivity ($1/\sigma$) of the individual CNF, which was calculated using the equation ($1/\sigma = l/RA$, where R is the electrical resistance in Ω, A is the cross-sectional area in cm^2, and l is the distance between electrodes in cm), displayed enhanced electrical conductivity from 1.29 to 4.28 $S\,cm^{-1}$. As the

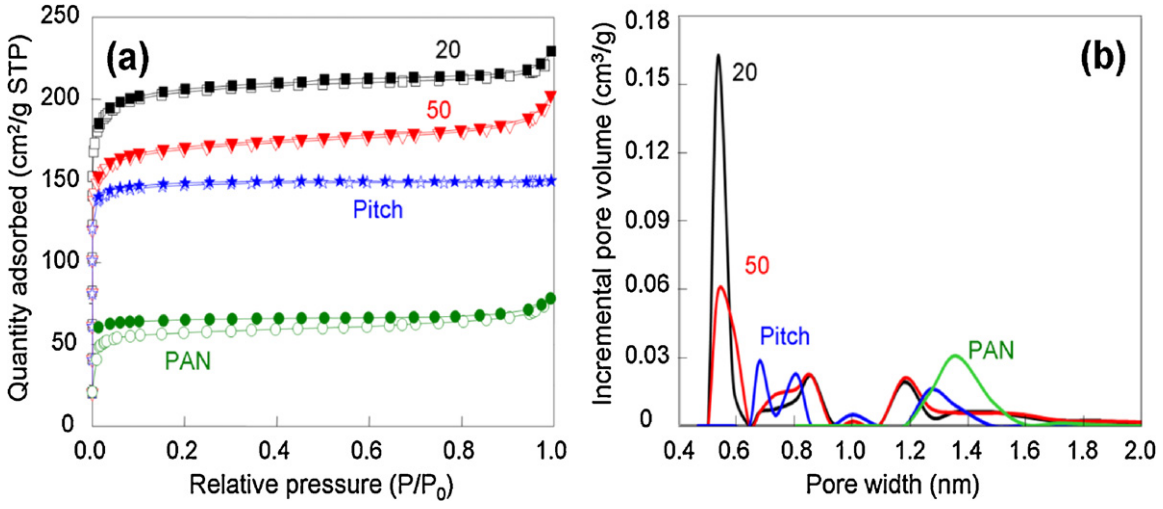

Fig. 3. (a) Nitrogen adsorption isotherms of the pure PAN- and the PAN/pitch-derived CNFs as a function of pitch concentration in THF and (b) pore size distribution calculated by the DFT method. Note that the blend ratio of PAN/pitch is constant at 7/3.

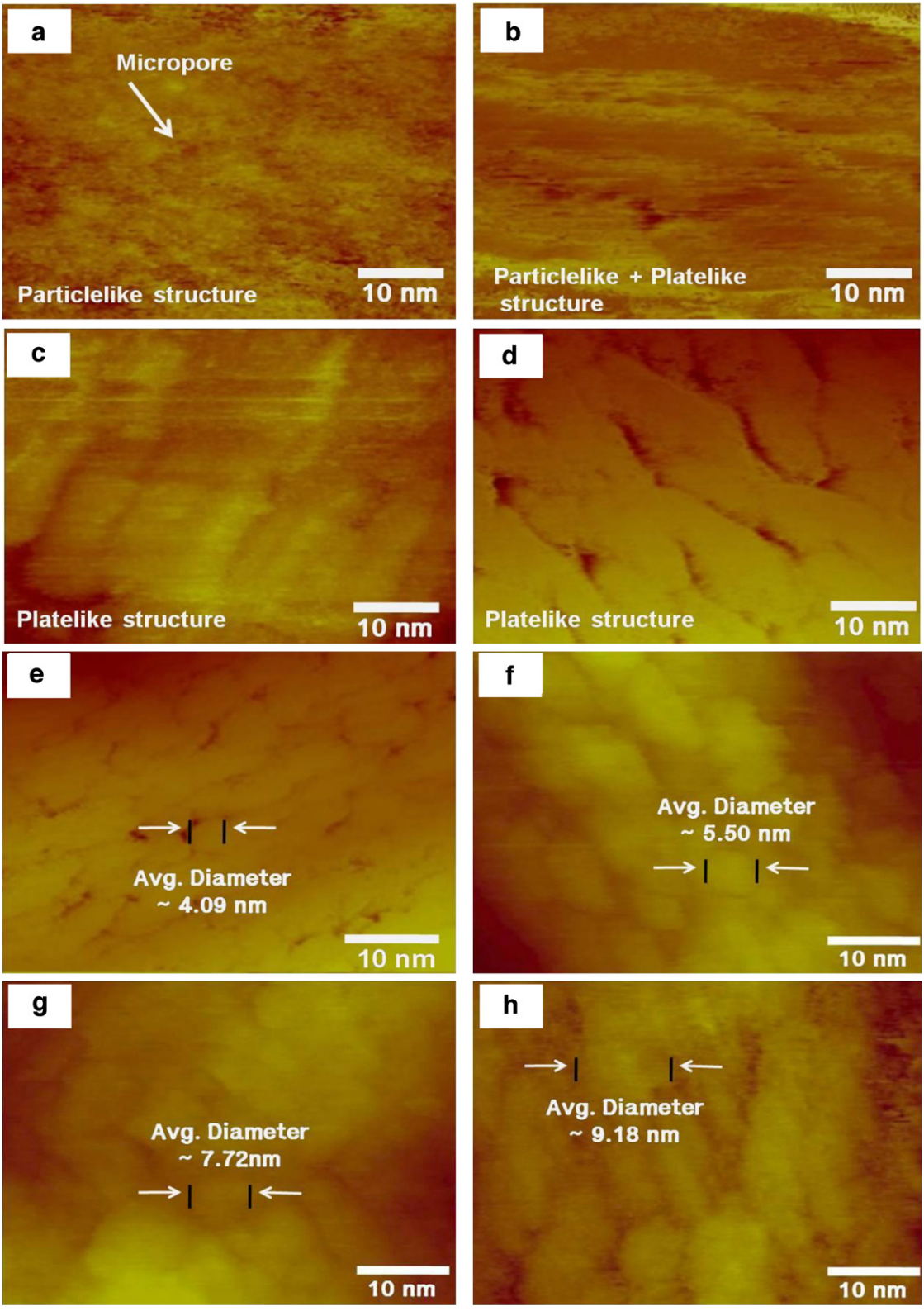

Fig. 4. STM images of PAN/pitch-derived CNFs (a) 20, (b) 30, (c) 40 wt.% pitch concentration, and (d) PAN-based CNF; high magnified STM images of (a–d) PAN/pitch-derived CNFs (a) 20, (b) 30, (c) 40, (d) 50 wt.% pitch concentration in THF.

amount of pitch increased, individual CNFs displayed enhanced electrical conductivity due to an increase in the degree of crystallinity of the pitch domain.

Surface area and pore size distribution of CNFs were characterized by nitrogen gas adsorption. The pore volumes in PAN/pitch-derived CNFs were mostly filled below $P/P_0 \approx 0.1$, indicating high microporosity (Fig. 3a). PAN-derived CNFs show type I isotherm (Fig. 3a) with high nitrogen uptakes at relatively low pressures characteristic of micropores with small amount of type IV mesopores behavior. The hysteresis loops obtained for PAN-derived

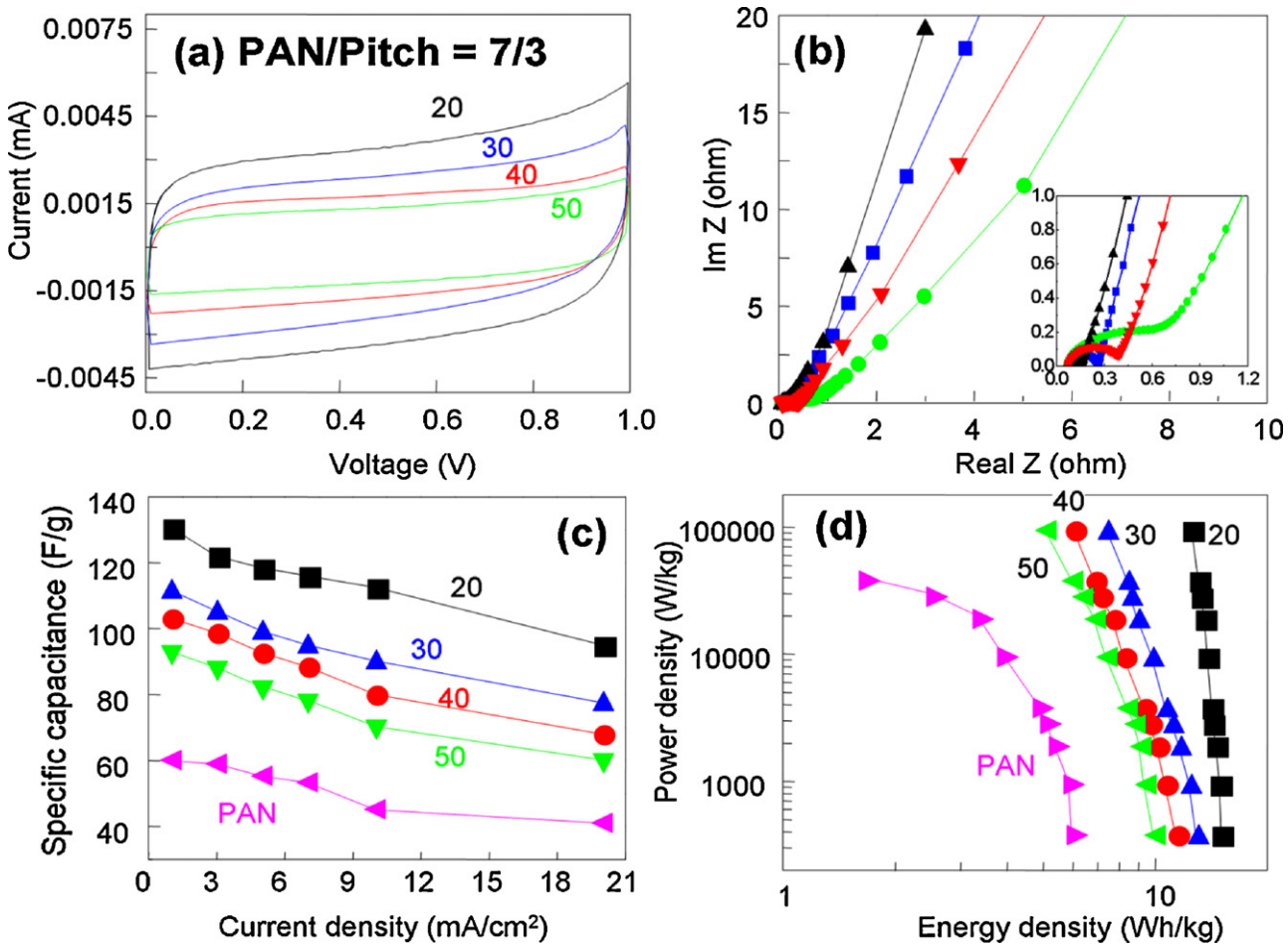

Fig. 5. (a) CVs in the range of 0–1.0 V obtained using a scan rate of 25 mV s^{-1}. (b) Complex-plane impedance plots. (c) Specific capacitances as a function of current density. (d) Ragone plots. (Note that value indicates the pitch concentration dissolved in THF.)

CNFs are typically attributed to narrow slit shaped pores including pores in the micropore region [12]. The pore size distributions of PAN/pitch-derived CNFs from DFT calculations exhibited narrow ultramicropores of less than 0.6 nm in Fig. 3b. In comparison, PAN-derived CNFs showed a broader distribution of micropore size with an average value of 1.4 nm. Therefore, PAN/pitch-derived CNFs are theoretically more suitable as electrode materials in an aqueous medium, because the ultramicropores in the carbon structure match well with the size of solvated ions (less than 1.0 nm) [13].

STM provides information on the domain size and microstructure of the domains of CNFs. As the pitch concentration increased, the shape of the surface changed from small particle-like to flat plate-like to large particle-like (Fig. 4a–d). The domain size of the CNFs derived from PAN/pitch increased with increasing the pitch concentration (Fig. 4e–h). Naturally, the larger domain size resulted in larger pores with smaller specific surface areas. The domain structures observed by STM were in agreement with the BET surface areas and pore size distributions. Therefore PAN/pitch-derived CNFs can be applied as efficient electrode materials for high-power supercapacitors because they have large accessible surface areas and relatively high electrical conductivities.

The resulting PAN/pitch-derived CNF web was cut into a rectangular shape (1.5 cm × 1.5 cm) and then attached to nickel plates to evaluate its capacitance based on a two-electrode system. The electrochemical properties of PAN/pitch-derived CNF webs were studied by CV in a 6 M KOH aqueous electrolyte solution. The data demonstrate that the electrodes are stable within the potential range (0–1.0 V) employed, and CV curves exhibit a good rectangular shape, representing energy storage by an electrical double layer mechanism in Fig. 5a. The capacitance decreased in proportion to the pitch concentration in THF, a pattern which is consistent with the specific surface area results. The electrochemical behavior of the electrodes could be more clearly understood by the impedance measurements. At high frequencies, small arcs were observed (see inset in Fig. 5b), indicating that the charge-transfer resistance between the electrode and the electrolyte was small; thus, the pore size of the carbon material was well-matched to the size of the electrolyte. Furthermore, the steep linear slopes at low frequencies indicated that the kinetics of ion diffusion in solution and the adsorption of ions onto the electrode surface were rapid. The ideal capacitance will give rise to a straight line along the imaginary axis at lower frequency. With decreasing the pitch concentration in THF, the pore density increased, which is why the capacitive behavior appeared at a lower resistance. Fig. 5c shows the change in the specific capacitance with increasing pitch concentration in as a function of the discharge current density ranging from 1 to 20 mA cm^{-2}. The specific capacitance decreased gradually with increasing discharge current density, indicating that the PAN/pitch-derived CNFs allowed rapid ion diffusion. We observed high specific capacitance (130.7 F g^{-1}) from the PAN/pitch (20 wt.% pitch concentration in THF)-derived CNF electrodes, which value is exactly twice as large as that of the PAN-based CNF electrodes. We conjecture that the pore size in PAN-derived CNFs, centered at 1.4 nm, was too large to accommodate the solvated ions effectively. The optimal match between pore size and the dimensions of the electrolyte allowed the PAN/pitch-derived CNFs electrode to

achieve high capacitance. Such a situation gives rise to enhanced capacitance, owing to the multiple interactions of the solvated ions with the pore of the carbon nanofiber [14]. In addition, according to the Ragone plot (Fig. 5d), both the fibrous morphology and the optimized pore sizes allow the PAN/pitch-derived CNF electrode to achieve both high energy density (ca. 15.0 Wh kg^{-1}) and high power density (ca. 100 kW kg^{-1}) simultaneously. The Ragone plot also shows that a high power density can be obtained without significant degradation in the energy density. The high power stability with PAN/pitch-derived CNFs is ascribed to their conductivity and to their structural/textural advantage.

4. Conclusion

We fabricate porous and small-sized fibrous carbon electrodes, in the form of a thin web, by electrospinning two immiscible polymer blends (PAN and pitch) followed by thermal treatment at 1000 °C in nitrogen. More specifically, the optimized selection of PAN/pitch blend allows us to synthesize CNFs, which exhibit a skin–core morphology. Simple thermal treatment of PAN/pitch-derived nanofibers creates suitable ultramicropores on the surface of CNFs that can accommodate many ions, removing the need for a time-consuming activation step. The pore sizes of the carbonized fiber can be selectively determined by the solution compositions, which will determine the phase behaviors depending on the concentrations of PAN/pitch in the solvent and the interaction parameters among them. These thin, flexible, and electrically conductive black webs, consisting of physically entangle long CNFs, enable us to fabricate highly pure and self-sustained electrodes without using binding or conductive materials. These electrodes can potentially be used in the fabrication of soft, portable electronic equipment, such as roll-up displays and wearable devices. Additionally, with their optimized micropores and large external surface area, PAN/pitch-derived porous CNF webs can store and deliver a large amount of ions at a high rate.

Acknowledgements

This work was supported by the National Research Foundation of Korea (NRF) Grant (NRF-2010-616-D00018) and the Ministry of Education, Science and Technology (MEST) (K20901001725-10E0100-09700). Y.A.K acknowledge the support from CLUSTER (the second stage) from the Ministry of Education, Culture, Sports, Science and Technology of Japan.

References

[1] B.E. Conway, Electrochemical Supercapacitors, Kluwer Academic, New York, 1999.
[2] P. Simon, Y. Gogotsi, Nat. Mater. 7 (2008) 845–854.
[3] S.R. Hwang, H. Teng, J. Electrochem. Soc. 149 (2002) A591–A596.
[4] K. Jurewicz, S. Delpeux, V. Bertagna, F. Beguin, E. Frackowiak, Chem. Phys. Lett. 347 (2001) 36–40.
[5] E. Frackowiak, F. Beguin, Carbon 39 (2001) 937–950.
[6] J.P. Zheng, P.J. Cygan, T.R. Jow, J. Electrochem. Soc. 142 (1995) 2699–2703.
[7] D.N. Futabe, K. Hata, T. Yamada, T. Hiraoka, Y. Hayamizu, Y. Kakudate, O. Tanaike, H. Atori, M. Yumura, A. Ijima, Nat. Mater. 5 (2006) 987–994.
[8] A. Chen, I. Minett, Y. Liu, C. Lynam, P. Sherrell, C. Wang, G.G. Wallace, Adv. Mater. 20 (2008) 566–570.
[9] C. Meng, C. Liu, S. Fan, Electrochem. Commun. 11 (2009) 186–189.
[10] J.S. Travis, A.R. Horst, Biomaterials 29 (2008) 1906–1989.
[11] S. Megelski, J.S. Stephens, D.B. Chase, J.F. Rabolt, Macromolecules 35 (2002) 8456–8466.
[12] K.S.W. Sing, D.H. Everett, R.A.W. Haul, L. Moscou, R.A. Pierotti, J. Rouquerol, T. Siemieniewska, Pure Appl. Chem. 57 (1985) 603–619.
[13] C.O. Ania, J. Pernak, F. Stefaniak, E. Raymundo-Piñero, F. Béguin, Carbon 47 (2009) 3158–3166.
[14] J. Chmiola, G. Yushin, Y. Gogotsi, C. Portet, P. Simon, P.L. Taberna, Science 313 (2006) 1760–1763.